Comparison of pressure profiles of massive relaxed galaxy clusters using the Sunyaev–Zel'dovich and x-ray data

2012 New J. Phys. 14 025010

(http://iopscience.iop.org/1367-2630/14/2/025010)

New Journal of Physics
The open-access journal for physics

Comparison of pressure profiles of massive relaxed galaxy clusters using the Sunyaev–Zel'dovich and x-ray data

Massimiliano Bonamente[1,2,12], Nicole Hasler[1], Esra Bulbul[1], John E Carlstrom[3,4,5], Thomas L Culverhouse[3], Megan Gralla[3], Christopher Greer[3], David Hawkins[6], Ryan Hennessy[3], Marshall Joy[2], Jeffery Kolodziejczak[2], James W Lamb[6], David Landry[1], Erik M Leitch[3], Daniel P Marrone[8], Amber Miller[9,10], Tony Mroczkowski[11], Stephen Muchovej[6], Thomas Plagge[3], Clem Pryke[3,4], Matthew Sharp[3] and David Woody[6]

[1] Department of Physics, University of Alabama, Huntsville, AL 35899, USA
[2] Space Science-VP62, NASA Marshall Space Flight Center, Huntsville, AL 35812, USA
[3] Kavli Institute for Cosmological Physics and the Department of Astronomy and Astrophysics, University of Chicago, Chicago, IL 60637, USA
[4] Enrico Fermi Institute, University of Chicago, Chicago, IL 60637, USA
[5] Department of Physics, University of Chicago, Chicago, IL 60637, USA
[6] Owens Valley Radio Observatory, California Institute of Technology, Big Pine, CA 93513, USA
[7] NASA Goddard Space Flight Center, Greenbelt, MD 20771, USA
[8] Steward Observatory, University of Arizona, 933 North Cherry Avenue, Tucson, AZ 85721, USA
[9] Columbia Astrophysics Laboratory, Columbia University, New York, NY 10027, USA
[10] Department of Physics, Columbia University, New York, NY 10027, USA
[11] Department of Physics and Astronomy, University of Pennsylvania, Philadelphia, PA 19104, USA
E-mail: bonamem@uah.edu

New Journal of Physics **14** (2012) 025010 (18pp)
Received 4 July 2011
Published 29 February 2012
Online at http://www.njp.org/
doi:10.1088/1367-2630/14/2/025010

[12] Author to whom any correspondence should be addressed.

Abstract. We present the Sunyaev–Zel'dovich (SZ) effect observations of a sample of 25 massive relaxed galaxy clusters observed with the Sunyaev–Zel'dovich array (SZA), an eight-element interferometer that is part of the Combined Array for Research in Millimeter-wave Astronomy (CARMA). We performed an analysis of new SZA data and archival *Chandra* observations of this sample to investigate the integrated pressure—a proxy for cluster mass—determined from x-ray and SZ observations, two independent probes of the intra-cluster medium (ICM). This analysis makes use of a model for the ICM introduced by Bulbul (2010 *Astrophys. J.* **720** 1038) which can be applied simultaneously to the SZ and x-ray data. With this model, we estimated the pressure profile for each cluster using a joint analysis of the SZ and x-ray data, and using the SZ data alone. We found that the integrated pressures measured from the x-ray and SZ data are consistent. This conclusion is in agreement with recent results obtained using *WMAP* and *Planck* data, confirming that SZ and x-ray observations of massive clusters detect the same amount of thermal pressure from the ICM. To test for possible biases introduced by our choice of model, we also fitted the SZ data using the universal pressure profile proposed by Arnaud (2010 *Astron. Astrophys.* **517** A92) and found consistency between the two models out to r_{500} in the pressure profiles and integrated pressures.

Contents

1. Introduction

The Sunyaev–Zel'dovich (SZ) effect (Sunyaev and Zel'dovich 1972) is a spectral distortion of the cosmic microwave background (CMB) caused by the scattering of CMB photons off the hot electrons of the intra-cluster medium (ICM). Over the last two decades, SZ observations with both single-dish and interferometric instruments have become routine (e.g. Birkinshaw *et al* 1991, Carlstrom *et al* 1996, Holzapfel *et al* 1997, Carlstrom *et al* 2002), and SZ surveys are now producing catalogues of newly discovered clusters out to high redshift (Vanderlinde

et al 2010, Marriage *et al* 2011, Williamson *et al* 2011, Planck Collaboration *et al* 2011a). SZ measurements are complementary to the x-ray measurements, which have long been used to study clusters, but only in recent years have sufficiently large samples of objects been observed in the SZ to permit a rigorous comparison between these two techniques (Reese *et al* 2002, Bonamente *et al* 2006, LaRoque *et al* 2006).

The SZ effect causes a perturbation ΔT of the CMB temperature $T_{\rm CMB}$ given by

$$\frac{\Delta T}{T_{\rm CMB}} = f(x) \int \sigma_{\rm T} n_{\rm e} \frac{k T_{\rm e}}{m_{\rm e} c^2} {\rm d}\ell = f(x) y, \tag{1}$$

where $f(x)$ is the frequency dependence of the SZ effect (e.g. LaRoque *et al* 2006); $\sigma_{\rm T}$ is the Thomson cross-section; $n_{\rm e}$, $T_{\rm e}$ and $m_{\rm e}$ are the number density, temperature and mass of the electrons, respectively; k is the Boltzmann constant; c is the speed of light; and the integral is along the line of sight ℓ. At a given frequency, the amplitude of the effect depends linearly on the Compton y-parameter, which is defined implicitly in equation (1). Note that the y-parameter is proportional to the ICM pressure integrated along the line of sight. At frequencies below 218 GHz, the SZ effect causes a decrement in the CMB temperature in the direction of the cluster. The integral of y over the solid angle Ω subtended by the cluster, known as the (cylindrical) integrated Compton y- parameter $Y_{\rm cyl} = \int y \, {\rm d}\Omega$, is expected to be a good proxy for cluster total mass since it traces the thermal energy content of the cluster gas. Alternatively, the Compton y- parameter can be integrated spherically,

$$Y_{\rm sph}(r_{500}) = \frac{1}{D_{\rm A}^2} \left(\frac{k \sigma_{\rm T}}{m_{\rm e} c^2} \right) \int n_{\rm e} T_{\rm e} \, {\rm d}V, \tag{2}$$

where the volume V is a sphere centered on the cluster and $D_{\rm A}$ is the angular diameter distance.

X-ray data can also be used to constrain the density and temperature—and thus the pressure—of the ICM. Over the last decade, several groups have investigated the consistency between x-ray and SZ pressure measurements. Early measurements of the SZ signal from *WMAP* by, e.g., Lieu *et al* (2006) and Bielby and Shanks (2007) detected an SZ signal at a lower level than expected. Atrio-Barandela *et al* (2008) showed that the isothermal beta model leads to an electron pressure profile that exceeds the measured values at large radii by a factor of few, and that the baryon profile is consistent with a model based on the Navarro *et al* (1997) matter profile. Diego and Partridge (2010) also showed that contamination by compact radio sources may have led to underestimates of the SZ effect flux decrements in the *WMAP* data. More recent comparisons of *Chandra* x-ray data to stacked data from *WMAP* and *Planck* (Melin *et al* 2011, Planck Collaboration *et al* 2011b) found consistency between SZ and x-ray measurements for large samples of clusters. Komatsu *et al* (2011) also analyzed a sample of massive nearby clusters individually resolved by *WMAP*, again finding good agreement with x-ray predictions.

In this paper, we present Sunyaev–Zel'dovich array (SZA) observations of the Allen *et al* (2008) sample of massive relaxed galaxy clusters, together with archival *Chandra* x-ray observations that are available for all clusters in this sample. The sensitivity and resolution of our data permit us to measure the pressure profile and the integrated pressure out to r_{500}—the radius within which the average cluster density is 500 times the critical density—for each cluster individually, without the need to resort to scaling relations between the x-ray luminosity and mass (as was done by Melin *et al* 2011, Planck Collaboration *et al* 2011b, for example). We use the Bulbul *et al* (2010) model of the cluster pressure, density and temperature. Since this model has a consistent parameterization for all thermodynamic quantities, it is especially well suited for joint x-ray and SZ analysis. As a cross-check against model-dependent biases, we also fit the

SZ data using the model of Arnaud *et al* (2010) based on the numerical simulations of Nagai *et al* (2007). We find consistency to within our measurement uncertainties both between the x-ray and SZ measurements and between the Bulbul *et al* (2010) and Arnaud *et al* (2010) models.

This paper is structured as follows: section 2 describes our observations and our sample, section 3 presents our joint analysis technique, section 4 describes our method of measuring the integrated $Y_{\rm sph}(r_{500})$ parameter (defined in equation (2)), section 5 presents and discusses our results, and our conclusions are presented in section 6.

2. Observations

The SZA is an eight-element interferometer designed for detecting and imaging the SZ effect from clusters at $z > 0.1$ and is part of the Combined Array for Research in Millimeter-wave Astronomy (CARMA). The array is equipped with 30 and 90 GHz receivers; all SZA observations presented in this paper were taken at 30 GHz. At this frequency, the 3.5 m diameter SZA telescopes have a field-of-view (or primary beam) of 10.′7 full-width at half-maximum (FWHM). Interferometric data are proportional to the Fourier transform of the sky brightness. These *visibility* data, denoted $V(u, v)$, are sampled at Fourier-plane coordinates (u, v) corresponding to the projected separation of pairs of telescopes (or *baselines*), as viewed by the source at the time of observation. At the time of the observations discussed in this work, the SZA antennas were arranged in a hybrid configuration, with six closely spaced telescopes and two 'outriggers' located ∼50 m from the inner array. The inner six telescopes probe small (u, v) Fourier modes, sampling the angular scales where the SZ signal is largest for moderate- to high-redshift clusters (1–6′). Baselines involving the outriggers are sensitive to angular scales down to ∼20″ and are used to constrain the positions and fluxes of unresolved radio sources.

Of the 42 clusters in the Allen *et al* (2008) sample of massive relaxed galaxy clusters, the SZA has observed the 31 objects above $\delta > -15^\circ$ at redshift $z \geqslant 0.09$. The declination restriction is imposed by the latitude of the observatory in the Owens Valley, California (37°14′02″N, 118°16′56″W), whereas the exclusion of clusters at low redshift is due to the inability of an interferometer to constrain scales larger than that which the shortest antenna spacing can probe at the lowest frequency band. The largest angular wavelength measured by the SZA is 10.9′, which for massive low-redshift clusters is generally smaller than $2r_{500}/D_{\rm A}$. Of these 31 clusters observed with the SZA, Abell 2390 and Abell 611 were excluded from this analysis because they did not have available local background in their *Chandra* ACIS-S x-ray observations. Three additional clusters—3C295, ClJ1415.2 + 3612 and Abell 963—were discarded because of extended or otherwise difficult-to-remove radio source contamination and one—RXJ0439.0 + 0521—because of a pointing error.

Our sample therefore consists of 25 clusters. The synthesized beam of the long (short) baseline data for this sample is approximately 15–30″ (90–180″), and the average rms noise in the maps is ∼ 0.25–0.30 mJy. In all cases, the *Chandra* data provide spatially resolved x-ray spectroscopy and sub-arcsecond imaging. A summary of the data is provided in table 1.

Radio sources detected in the cluster fields are reported in table 2. For each cluster field, we use the NRAO VLA Sky Survey (NVSS) and Faint Images of the Radio Sky at Twenty-centimeters (FIRST) 1.4 GHz catalogues as a reference for locating compact radio sources within 10′ of the cluster center. Most radio sources in our observations have counterparts in the FIRST survey, which has an rms noise of 0.15 mJy at 1.4 GHz. Inverted spectrum sources that may be present at 30 GHz may not have counterparts at 1.4 GHz, but fortunately they constitute a small fraction of the source population (Muchovej *et al* 2010).

Table 1. Sample of massive and relaxed clusters from the Allen *et al* (2008) sample with high-resolution SZ effect SZA observations.

Cluster	z	R.A. (J2000)	Dec. (J2000)	N_H (10^{20} cm^{-2})[a]	SZA (h)[b]	ACIS	*Chandra* ObsID	(ks)[c]
MACSJ0159.8 − 0849	0.40	01 59 49.5	−08 50 02	2.06	21.2	I	3265	16.4
						I	6106	34.3
						I	9376	19.5
Abell 383	0.19	02 48 03.4	−03 31 44	3.40	25.0	I	524	9.9
						I	2320	18.5
MACSJ0329.7 − 0212	0.45	03 29 41.7	−02 11 48	3.43	8.1	I	6108	32.7
						I	3257	9.6
						I	3582	19.3
Abell 478	0.09	04 13 25.2	+10 27 52	34.29	37.1	I	6102	10.0
MACSJ0429.6 − 0253	0.40	04 29 36.1	−02 53 08	3.23	22.1	I	3271	23.2
3C186	1.06	07 44 17.5	+37 53 17	5.11	13.7	S	9407	66.3
						S	9408	39.6
						S	9774	75.1
						S	9775	15.9
MACSJ0744.9 + 3927	0.69	07 44 52.9	+39 27 26	5.66	12.7	I	6111	49.5
						I	3197	20.2
						I	3585	19.7
MACSJ0947.2 + 7623	0.34	09 47 13.1	+76 23 14	2.28	11.5	I	2202	11.7
Zwicky 3146	0.29	10 23 39.6	+04 11 10	2.46	6.8	I	909	45.2
						I	9371	36.3
MACSJ1115.8 + 0129	0.35	11 15 52.0	+01 29 58	4.34	26.2	I	9375	39.6
MS 1137.5 + 6625	0.78	11 40 22.2	+66 08 14	0.95	19.6	I	536	109.6
Abell 1413	0.14	11 55 18.2	+23 24 19	3.60	43.2	I	5003	66.6
						I	1661	9.1
						I	5002	34.4
ClJ1226.9+3332	0.89	12 26 58.2	+33 32 47	1.83	16.0	I	5014	31.6
						I	3180	29.9
MACSJ1311.0 − 0311	0.49	13 11 01.7	−03 10 38	1.82	4.6	I	6110	63.0
						I	3258	13.1
						I	9381	29.0
RXJ1347.5 − 1145	0.45	13 47 30.6	−11 45 10	4.60	25.7	I	3592	54.8
Abell 1835	0.25	14 01 02.0	+02 52 40	2.04	9.0	I	6880	117.9
						I	6881	36.8
						I	7370	40.0
MACSJ1423.8 + 2404	0.54	14 23 47.9	+24 04 42	2.20	6.5	I	1657	18.2
MACSJ1427.3 + 4408	0.49	14 27 16.3	+44 07 29	1.19	17.4	I	6112	8.8
						I	9380	25.8
						I	9808	14.9
RXJ1504.1 − 0248	0.21	15 04 07.5	− 02 48 16	5.97	9.2	I	5793	39.2
						I	4935	11.9
MACSJ1532.9 + 3021	0.36	15 32 53.8	+30 20 58	2.30	14.6	I	1665	8.2

Table 1. Continued.

Cluster	z	R.A. (J2000)	Dec. (J2000)	N_H (10^{20} cm^{-2})[a]	SZA (h)[b]	ACIS	*Chandra* ObsID	(ks)[c]
MACSJ1621.6+3810	0.46	16 21 24.9	+38 10 08	1.13	44.0	I	6172	29.2
						I	3254	9.6
						I	6109	36.7
						I	9379	29.7
						I	10785	29.7
Abell 2204	0.15	16 32 46.9	+05 34 31	5.67	19.6	I	7940	76.9
MACSJ1720.3+3536	0.39	17 20 16.8	+35 36 25	3.46	36.2	I	6107	29.1
						I	3280	20.6
						I	7718	7.0
RXJ2129.6+0005	0.23	21 29 40.0	+00 05 18	3.63	24.5	I	552	10.0
Abell 2537	0.29	23 08 22.2	−02 11 28	4.62	24.8	I	9372	38.5

[a] N_H is the HI Galactic column density.
[b] SZA exposure is unflagged, on-source time.
[c] *Chandra* exposure is unflagged, on-source time.

For all 25 clusters in our sample, we have available archival *Chandra* x-ray observations (Allen *et al* 2008). Event files for all cluster observations and additional blank-sky composite event files used for background subtraction were reduced using CIAO 4.3.1 and CALDB 4.3. X-ray spectra are extracted in several annular regions for each cluster, centered at the peak of the x-ray emission. Emphasis is placed on the removal of periods of high background, and on the modeling of soft x-ray residuals that may be present after the subtraction of the blank-sky background. The method of analysis of the *Chandra* data and examples of the temperature and surface brightness profiles can be found in Bulbul *et al* (2010) and Hasler *et al* (2011). More details of the *Chandra* data for all clusters in this sample will be given in a forthcoming paper in which we will present the measurement of the gas mass fraction from the x-ray observations.

In figure 1, we show the raw *Chandra* x-ray images (binned in the 0.7–7 keV energy band) for each of the 25 clusters, with contours obtained from the short baseline point source-removed SZA data overlaid.

3. Analysis of the Sunyaev–Zel'dovich array and *Chandra* data

3.1. Models for the thermodynamic quantities

We analyze the SZ and x-ray data using the Bulbul *et al* (2010) model, which uses a consistent parameterization of the electron density, temperature and pressure, related through the ideal gas law at all radii, i.e. $p_e(r) = n_e(r)kT_e(r)$ for pressure p_e, electron density n_e and temperature T_e. All thermodynamic quantities depend on the gravitational potential,

$$\phi(r) = \left[\frac{1}{(\beta-2)}\frac{(1+r/r_s)^{\beta-2}-1}{r/r_s(1+r/r_s)^{\beta-2}}\right], \tag{3}$$

Table 2. SZ centroids and radio source locations for the SZA observations.

		SZ centroid			30 GHz source			1.4 GHz Flux (mJy)	
Cluster	z	α(J2000)	δ(J2000)	src	$\Delta\alpha$ ($''$)[a]	$\Delta\delta$ ($''$)[a]	Flux (mJy)	NVSS	FIRST
MACSJ0159.8 − 0849	0.40	01:59:51.5	−08:50:06.9	1	−31.3	8.0	84.4 ± 0.2	36.7	31.4
Abell 383	0.19	02:48:03.5	−03:31:55.8	1	−1.5	11.5	4.3 ± 0.2	40.9	–
				2	276.7	−149.2	7.5±0.3	54.9	–
MACSJ0329.7 − 0212	0.45	03:29:40.3	−02:11:44.5	1	263.2	−97.2	12.7 ± 0.4	37.2	–
Abell 478	0.09	04:13:25.0	+10:27:50.8	1	195.4	18.1	2.9 ± 0.1	47.7	–
				2	3.3	4.1	2.3±0.1	36.9	–
MACSJ0429.6 − 0253	0.40	04:29:35.6	−02:53:01.6	1	7.0	−7.7	18.2 ± 0.2	138.8	–
				2	−285.4	53.9	3.2 ± 0.2	18.3	–
3C186	1.06	07:44:14.8	+37:53:21.2	1	40.8	−3.3	22.6 ± 0.2	1236.4	1244.9
				2	81.6	−94.3	10.6 ± 0.2	105.4	49.2
MACSJ0744.9 + 3927	0.69	07:44:52.2	+39:27:34.6	1	−215.6	286.7	2.5 ± 0.5	–	4.4
MACSJ0947.2 + 7623	0.34	09:47:12.4	+76:23:03.0	1	11.1	11.2	2.5 ± 0.3	21.7	–
Zwicky 3146	0.29	10:23:38.9	+04:11:27.7	1	92.4	−48.5	5.0 ± 0.3	95.8	56.7
				2	8.9	−17.6	1.7 ± 0.2	7.1	2.0
				3	−46.2	−138.7	2.2 ± 0.2	31.5	15.1
MACSJ1115.8 + 0129	0.35	11:15:52.2	+01:29:50.6	1	128.7	−360.5	2.7 ± 0.2	11.5	10.5
				2	162.2	−95.5	3.7 ± 0.2	–	2.1
				3	139.7	−64.8	1.8 ± 0.3	–	–
				4	−3.1	3.0	1.4 ± 0.4	6.2	5.6
				5	−168.9	−71.2	2.7 ± 0.2	10.3	6.4
MS1137.5 + 6625	0.78	11:40:22.8	+66:08:13.2	–	–	–	–	–	–
Abell 1413	0.14	11:55:17.5	+23:24:04.0	1	−117.0	135.5	2.1 ± 0.1	28.1	19.8
				2	−386.0	−185.2	2.8 ± 0.3	–	–
CLJ1226.9 + 3332	0.89	12:26:57.7	+33:32:51.8	1	263.4	−46.0	3.9 ± 0.2	29.8	23.2
MACSJ1311.0 − 0311	0.49	13:11:02.2	−03:10:47.0	–	–	–	–	–	–
RXJ1347.5 − 1145	0.45	13:47:31.4	−11:45:16.1	1	−11.4	6.3	8.7 ± 0.2	45.9	–
				2	−339.1	251.5	6.9 ± 0.4	365.8	–
				3	−53.3	279.5	2.6 ± 0.3	5.1	–
Abell 1835	0.25	14:01:02.2	+02:52:34.4	1	−1.5	9.2	2.9 ± 0.3	39.3	31.3
				2	−29.0	−47.7	1.0 ± 0.3	–	–
MACSJ1423.8 + 2404	0.54	14:23:48.6	+24:05:13.6	1	−11.8	−31.5	2.0 ± 0.2	8.0	5.2
MACSJ1427.3 + 4408	0.49	14:27:15.8	+44:07:41.4	1	4.8	−10.8	16.4 ± 0.2	47.9	41.3
				2	33.6	206.8	1.1 ± 0.2	8.6	8.2
RXJ1504.1 − 0248	0.21	15:04:07.1	−02:48:17.8	1	5.7	1.3	15.9 ± 0.2	60.5	40.8
MACSJ1532.9 + 3021	0.36	15:32:54.0	+30:20:59.0	1	−39.3	−72.9	5.7 ± 0.2	7.9	6.0
				2	−2.7	0.3	3.2 ± 0.2	22.8	15.2
				3	−82.8	−128.4	1.3 ± 0.2	18.0	4.1
MACSJ1621.6 + 3810	0.46	16:21:25.3	+38:09:56.9	–	–	–	–	–	–
Abell 2204	0.15	16:32:47.2	+05:34:34.7	1	−3.6	−1.5	7.0 ± 0.2	69.3	57.9
				2	−421.8	−362.8	21.6 ± 0.2	41.6	–
				3	191.0	−132.8	0.7 ± 0.1	12.2	1.2
MACSJ1720.3 + 3536	0.39	17:20:16.2	+35:36:36.0	1	650.3	340.2	167.7 ± 0.2	–	–
				2	10.3	−9.4	1.8 ± 0.4	18.0	16.8
RXJ2129.6 + 0005	0.23	21:29:40.2	+00:05:20.9	1	−3.2	0.4	2.6 ± 0.2	25.4	23.8
				2	228.1	160.9	3.1 ± 0.2	34.3	6.6
Abell 2537	0.29	23:08:19.2	−02:11:19.0	1	138.6	437.2	8.4 ± 0.9	69.9	58.6

[a] Offset from fit SZ centroid.

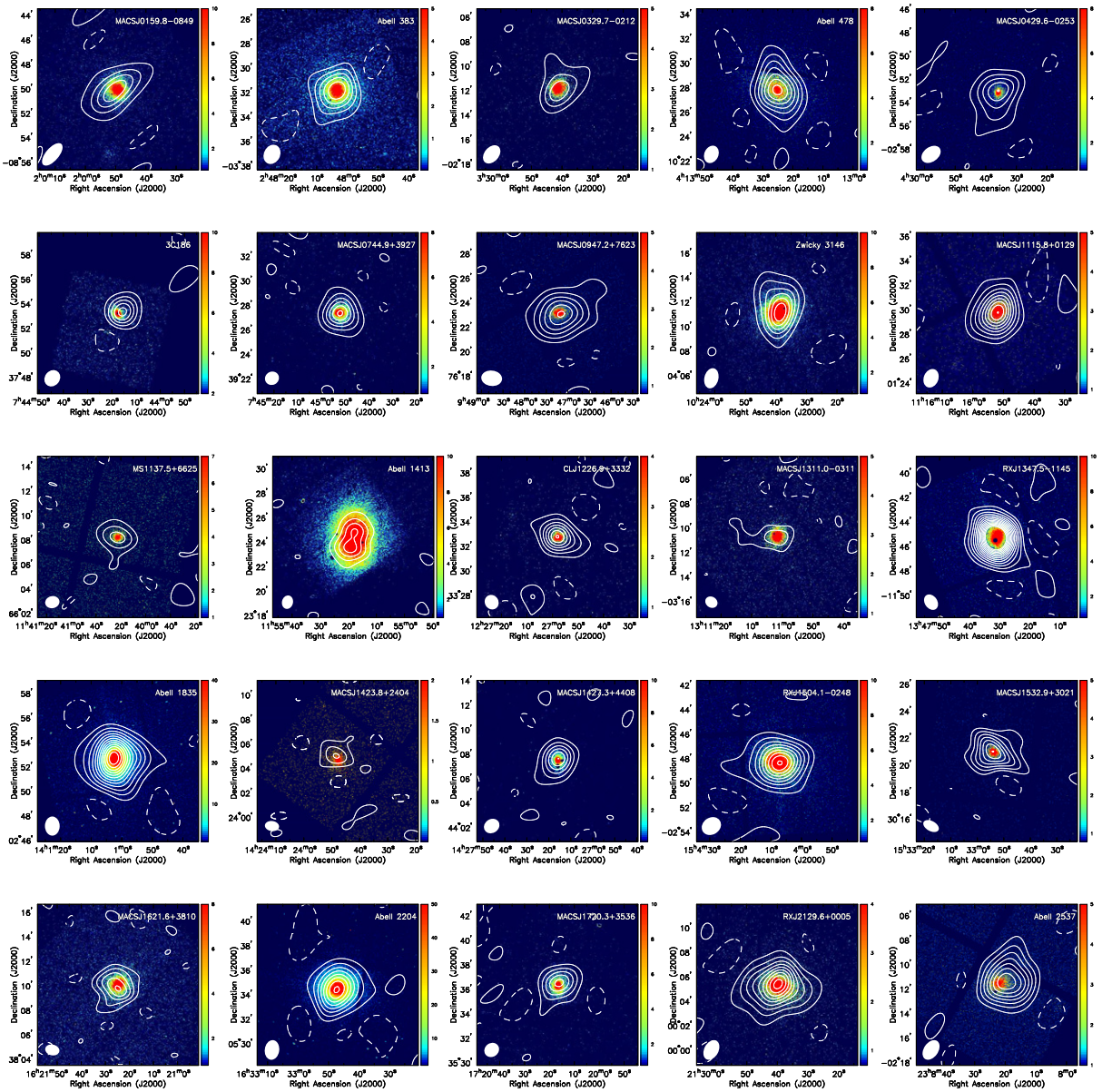

Figure 1. *Chandra* images in the 0.7–7 keV energy range. The color bars reflect the number of counts detected by *Chandra*. SZ contour levels are (+2, −2, −4, −6, −8, ...) times the rms noise in the short baseline data, after removal of radio sources; solid contours are for negative levels, and dashed contours are for positive levels. The elliptical Gaussian approximation to the synthesized beam of the SZ observations is shown in the lower left corner.

in which β describes the slope of the matter density at large radii and r_s is a scale radius. The parameterization of the Bulbul *et al* (2010) model does not allow the inner slope of the matter density to vary, which is fixed at r^{-1} as in the Navarro *et al* (1997) model. The resolution of our SZ data can only effectively constrain the matter distribution on scales larger than the synthesized beam, which is of the order of 1 arcmin for these observations, and therefore we

would not be able to place significant constraints on the inner slope. As explained by Bulbul *et al* (2010), the potential is continuous at $\beta = 2$, the value of the Navarro *et al* (1997) mass density model. The radial electron temperature profile is given by

$$T_{\rm e}(r) = T_0 \phi(r) \tau_{\rm cool}(r), \tag{4}$$

where $\tau_{\rm cool}(r)$ is the Vikhlinin *et al* (2006) phenomenological core taper function, required to fit cool-core clusters, which is equal to one at large radii. The density is parameterized as

$$n_{\rm e}(r) = n_{\rm e0} \phi(r)^n \tau_{\rm cool}^{-1}(r) \tag{5}$$

in such a way that the pressure distribution is not altered by the presence of the cool core. At large radii, where the effect of the cool core vanishes, the thermodynamic quantities are related by a simple polytropic equation of state. The electron pressure profile is therefore parameterized as

$$p_{\rm e}(r) = P_{\rm e0} \phi(r)^{n+1} \tag{6}$$

and is independent of the presence of a cool core. The model therefore has five independent parameters for non-cool-core clusters: the scale radius $r_{\rm s}$, the index β, the polytropic index n and the normalization constants for the three thermodynamic quantities which satisfy $n_{\rm e0} k T_0 = P_{\rm e0}$. For cool-core clusters, the $\tau_{\rm cool}$ function

$$\tau_{\rm cool}(r) = \frac{\alpha + (r/r_{\rm cool})^\gamma}{1 + (r/r_{\rm cool})^\gamma} \tag{7}$$

adds three additional adjustable parameters.

To test for model-dependent biases, we also use the Arnaud *et al* (2010) model to fit the SZ data. This model describes the cluster pressure profile using an analytic function motivated by numerical simulations (Nagai *et al* 2007) and x-ray observations of the REXCESS sample,

$$p_{\rm e}(r) = \frac{p_{{\rm e},i}}{(r/r_p)^c \left[1 + (r/r_p)^a\right]^{(b-c)/a}}. \tag{8}$$

The parameters $p_{{\rm e},i}$ and r_p are left free in our fits to the SZ effect observations. The values (a, b, c) are the power-law indices that describe the (intermediate, outer and inner) slopes of $p_{\rm e}(r)$. We use the 'universal' values $(a, b, c) = (1.05, 5.49, 0.31)$ obtained by Arnaud *et al* (2010) from a fit to x-ray observations of the REXCESS sample. Note that Arnaud *et al* (2010) found different best-fit values for cool-core clusters. We choose to use the parameters fit to the entire sample because our sample was not selected based on the presence of a cool core and in fact contains a few non-cool-core clusters, namely 3C186, MS1137.5 + 6625 and CLJ1226.9 + 3332.

3.2. Method of analysis

As in previous work with the SZA (e.g. Mroczkowski *et al* 2009, Hasler *et al* 2011), we relate the point-source-subtracted interferometric SZ visibilities to the unitless integrated Compton y by introducing $Y(u, v)$, defined as

$$Y(u, v) \equiv \frac{V_\nu(u, v)}{g(x)\, I_0}. \tag{9}$$

Here $g(x)$ corrects for the frequency dependence of the SZ flux, and $I_0 = 2(k_{\rm B} T_{\rm CMB})^3/(hc)^2$ is the primary CMB intensity. The SZ models and compact radio sources are fit directly and

simultaneously in Fourier space, where the statistical properties of the model fits are better understood and the noise is Gaussian. This is done simply by building up the sky brightness image, Fourier transforming it, and computing the likelihood of the model.

The x-ray data consist of spectroscopic temperature measurements taken in cluster-centric annuli, and an x-ray image in units of surface brightness (counts $s^{-1}\,cm^{-2}\,sr^{-1}$). The x-ray surface brightness S_x varies with the line of sight integral of the electron density and temperature distributions as

$$S_x = \frac{1}{4\pi(1+z)^3}\int n_e^2 \Lambda_{ee}(T_e, A)\mathrm{d}\ell, \tag{10}$$

where ℓ is the line of sight through the cluster, n_e is the electron density, T_e is the electron temperature, A is the metallicity and $\Lambda_{ee}(T_e, A)$ is the x-ray cooling function (in units of counts $cm^3\,s^{-1}$) as a function of electron temperature and metallicity. Each cluster was divided into a number of annuli according to the total number of photons detected, and for each annular region the temperature and abundance were free parameters. The surface brightness is only marginally sensitive to the choice of the outer limit of integration in equation (10): we find that the masses vary by less than 1% when the outer limit ranges between 2 and 5 Mpc. We therefore choose a limit of 2 Mpc, which corresponds to approximately the virial radius for clusters in this mass range. We use the Mazzotta *et al* (2004) definition of spectroscopic temperature in the comparison of model and observed temperatures in each annulus.

We first estimate the pressure profile of the ICM by jointly fitting the SZ and x-ray data with the Bulbul *et al* (2010) model. Both datasets are used simultaneously to constrain all three thermodynamic quantities, with the global shape parameters β, n and r_s (and the cool-core parameters when applicable) linked among the profiles. Both datasets contribute to the determination of the shape of the pressure profile, with SZ observations contributing primarily at the largest radii where the sensitivity of *Chandra* to the diffuse cluster emission is limited. Instead of linking the normalization of the pressure profile (P_{e0}) to the product of the normalizations of the density and temperature (n_{e0} and T_0), we let the normalizations be free, and check *a posteriori* that $P_{e0} = n_{e0} \times kT_0$ in accordance with the ideal gas law. The normalization of the pressure is determined by the SZ data, and the normalizations of temperature and density are determined by the x-ray data.

This method results in the measurement of the shape of the pressure profile, $p_e(r)/P_{e0}$, and two normalizations determined independently by each of the two datasets. The two normalizations are left free to vary, because in principle systematic uncertainties in the two datasets could lead to different values, and we do not want to assume *a priori* agreement between them. The fit uses a Markov chain Monte Carlo method (Bonamente *et al* 2004) and computes the angular diameter distance assuming a $\Omega_\Lambda = 0.73$, $\Omega_M = 0.27$ and $h = 0.73$ cosmology.

To obtain a measurement of the integrated pressure that depends only on the SZ data, we also perform another fit in which we fix the shape parameters of the Bulbul *et al* (2010) pressure profile to $n = 3.5$ and $\beta = 2.0$. These values correspond to the median of the values obtained from the joint fit. This pressure profile with fixed slope parameters is directly comparable to the universal pressure profile of Arnaud *et al* (2010), since both are determined by the modeling of high-resolution x-ray data (from fits to the REFLEX sample for the Arnaud *et al* 2010 model and from fits to the Allen *et al* 2008 observations for our model), and have just two free parameters (scale radius and normalization constant). In the following, we refer to this two-parameter model as the Bulbul *et al* (2010) average pressure profile.

Measurements of the ICM pressure using SZ and x-ray data are subject to different sources of systematic uncertainty that could affect the calculation of the $Y_{\rm sph}$ parameter (Hasler *et al* 2011). Systematic errors that integrate down with sample size include cluster asphericity, the effect of x-ray background and the presence of the kinetic SZ effect; these errors are included in the calculation of the ratio between the various measurements of $Y_{\rm sph}(r_{500})$, and of the weighted averages and $\chi^2_{\rm min}$ values in sections 4.1 and 4.2, following the prescriptions of Hasler *et al* (2011).

4. Integrated pressure measurements

4.1. Joint Sunyaev–Zel'dovich (SZ) and x-ray fit using the Bulbul et al (2010) model

The integrated pressure, which we quantify in terms of the Compton y parameter, is expected to be a good proxy for total cluster mass. Since the SZA measures the integrated flux within Fourier modes on the sky, our SZ data relate most directly to the integrated Compton y parameter $Y_{\rm cyl}$. However, it is conventional in x-ray analyses to report spherically integrated quantities. We therefore quantify the integrated pressure using the spherically integrated Compton y parameter $Y_{\rm sph}$ out to r_{500}. The overdensity radius r_{500} is given by

$$r_\Delta = \left(\frac{M_{\rm tot}(r_\Delta)}{\frac{4}{3}\pi \cdot \Delta \rho_{\rm c}(z)} \right)^{1/3} \tag{11}$$

with $\Delta = 500$, where $\rho_{\rm c}(z)$ is the critical density of the universe at the cluster redshift. The total cluster mass is calculated under the assumption of hydrostatic equilibrium; for the Bulbul *et al* (2010) model, the total mass is given by

$$M_{\rm tot}(r) = \frac{4\pi \rho_i r_{\rm s}^3}{(\beta - 2)} \left(\frac{1}{\beta - 1} + \frac{1/(1-\beta) - r/r_{\rm s}}{(1 + r/r_{\rm s})^{\beta - 1}} \right) \tau_{\rm cool}(r), \tag{12}$$

where the matter density normalization is given by $\rho_i = (kT_0(n+1)(\beta-1))/(4\pi G \mu m_{\rm p} r_{\rm s}^2)$; μ is the mean molecular weight and $m_{\rm p}$ is the proton mass.

Using the method of analysis discussed in section 3.2, we first compare $Y_{\rm sph}$ normalized using $n_{\rm e0}$ and T_0 constrained by the x-ray data with $Y_{\rm sph}$ normalized using $P_{\rm e0}$ constrained by the SZ data. This comparison is summarized in table 3. The normalizations are in good agreement: the weighted average of the ratio between the measurements using the SZ and x-ray normalizations is 1.06 ± 0.04. This indicates that systematic uncertainties do not produce a large overall offset between the two observables.

Below, we refer to $Y_{\rm sph}$ as the measurement obtained from the joint fit using the x-ray normalization. We adopt this value since the joint profile makes use of all the information available from both the x-ray and SZ observations including the effect of the cool core, and since both normalizations are in agreement.

4.2. SZ-only fit using the Bulbul et al (2010) average pressure profile

We also fit only the SZA data to the Bulbul *et al* (2010) average pressure profile, which consists of the pressure profile of equation (6) with $P_{\rm e0}$ and $r_{\rm s}$ as free parameters and the two shape parameters fixed at $n = 3.5$ and $\beta = 2.0$. We use this model to compute Y as described above, which we refer to as $Y_{\rm sph,SZ,B10}$. The value of r_{500} used in computing $Y_{\rm sph,SZ,B10}$ is determined

Table 3. Measurement of integrated $Y_{\rm sph}$ at r_{500} from joint x-ray and SZ data using the polytropic model.

		$Y_{\rm sph}(r_{500})$		
Cluster	$r_{500}(')$	SZ normalization (10^{-11})	x-ray normalization (10^{-11})	SZ to x-ray ratio
MACSJ0159.8 − 0849	$221.1\pm^{11.0}_{12.3}$	$8.30\pm^{0.76}_{0.88}$	$9.67\pm^{1.14}_{1.12}$	$0.86\pm^{0.08}_{0.07}$
Abell 383	$268.5\pm^{22.1}_{20.7}$	$4.92\pm^{0.77}_{0.70}$	$4.19\pm^{0.82}_{0.70}$	$1.17\pm^{0.16}_{0.15}$
MACS0329.7 − 0212	$138.4\pm^{12.7}_{11.9}$	$3.03\pm^{0.53}_{0.49}$	$2.61\pm^{0.59}_{0.49}$	$1.16\pm^{0.20}_{0.18}$
Abell 478	$714.3\pm^{23.5}_{34.5}$	$49.61\pm^{3.15}_{3.19}$	$60.62\pm^{4.84}_{6.13}$	$0.82\pm^{0.06}_{0.05}$
MACSJ0429.6 − 0253	$182.3\pm^{18.5}_{15.1}$	$2.75\pm^{0.49}_{0.43}$	$3.30\pm^{0.81}_{0.61}$	$0.83\pm^{0.14}_{0.14}$
3C186	$72.1\pm^{5.5}_{5.7}$	$1.01\pm^{0.23}_{0.20}$	$0.86\pm^{0.14}_{0.13}$	$1.17\pm^{0.24}_{0.21}$
MACSJ0744.9 + 3927	$120.3\pm^{8.6}_{7.5}$	$5.04\pm^{0.66}_{0.57}$	$3.80\pm^{0.72}_{0.57}$	$1.33\pm^{0.16}_{0.15}$
MACSJ0947.2 + 7623	$196.2\pm^{15.1}_{15.5}$	$5.18\pm^{0.73}_{0.70}$	$6.00\pm^{1.17}_{1.11}$	$0.86\pm^{0.14}_{0.11}$
Zwicky 3146	$265.7\pm^{8.7}_{8.6}$	$12.17\pm^{1.22}_{1.17}$	$10.56\pm^{0.93}_{0.95}$	$1.14\pm^{0.13}_{0.10}$
MACSJ1115.8 + 0129	$200.0\pm^{9.6}_{10.7}$	$7.74\pm^{0.57}_{0.58}$	$6.26\pm^{0.78}_{0.83}$	$1.24\pm^{0.14}_{0.11}$
MS1137.5 + 6625	$78.8\pm^{5.6}_{5.1}$	$1.08\pm^{0.16}_{0.15}$	$0.73\pm^{0.11}_{0.10}$	$1.49\pm^{0.26}_{0.24}$
Abell 1413	$454.4\pm^{20.3}_{20.3}$	$17.10\pm^{2.64}_{2.03}$	$23.12\pm^{2.36}_{2.32}$	$0.75\pm^{0.07}_{0.06}$
CLJ1226.9 + 3332	$109.4\pm^{8.3}_{8.3}$	$3.31\pm^{0.34}_{0.34}$	$3.06\pm^{0.54}_{0.52}$	$1.09\pm^{0.18}_{0.15}$
MACSJ1311.0 − 0311	$156.5\pm^{11.5}_{10.2}$	$2.36\pm^{0.61}_{0.58}$	$2.31\pm^{0.36}_{0.31}$	$1.02\pm^{0.26}_{0.23}$
RXJ1347.5 − 1145	$218.0\pm^{6.6}_{5.9}$	$14.02\pm^{0.75}_{0.75}$	$21.59\pm^{1.82}_{1.82}$	$0.65\pm^{0.04}_{0.04}$
Abell 1835	$370.7\pm^{7.6}_{8.0}$	$31.41\pm^{1.56}_{1.56}$	$29.67\pm^{1.56}_{1.57}$	$1.06\pm^{0.06}_{0.06}$
MACSJ1423.8 + 2404	$189.1\pm^{16.4}_{15.4}$	$2.15\pm^{0.45}_{0.39}$	$2.52\pm^{0.57}_{0.51}$	$0.86\pm^{0.22}_{0.18}$
MACSJ1427.3 + 4408	$150.5\pm^{4.2}_{4.6}$	$3.39\pm^{0.57}_{0.50}$	$4.75\pm^{0.44}_{0.46}$	$0.72\pm^{0.11}_{0.11}$
RXJ1504.1 − 0248	$326.7\pm^{12.1}_{9.9}$	$15.73\pm^{1.43}_{1.30}$	$18.03\pm^{1.54}_{1.26}$	$0.87\pm^{0.06}_{0.06}$
MACSJ1532.9 + 302	$189.1\pm^{9.9}_{9.1}$	$5.04\pm^{0.65}_{0.55}$	$4.61\pm^{0.61}_{0.50}$	$1.09\pm^{0.12}_{0.12}$
MACSJ1621.6 + 3810	$147.7\pm^{8.0}_{11.1}$	$2.53\pm^{0.29}_{0.30}$	$2.76\pm^{0.37}_{0.48}$	$0.93\pm^{0.12}_{0.10}$
Abell 2204	$504.6\pm^{12.5}_{11.2}$	$44.97\pm^{2.99}_{2.74}$	$43.93\pm^{3.08}_{2.59}$	$1.02\pm^{0.05}_{0.05}$
MACSJ1720.3 + 3536	$170.5\pm^{8.6}_{8.1}$	$3.89\pm^{0.30}_{0.29}$	$3.93\pm^{0.49}_{0.42}$	$0.98\pm^{0.10}_{0.09}$
RXJ2129.6 + 0005	$297.6\pm^{13.1}_{13.6}$	$10.78\pm^{1.04}_{1.02}$	$10.48\pm^{1.34}_{1.22}$	$1.04\pm^{0.10}_{0.11}$
Abell 2537	$256.2\pm^{13.4}_{14.4}$	$7.27\pm^{0.81}_{0.77}$	$7.37\pm^{0.97}_{0.95}$	$0.99\pm^{0.09}_{0.09}$

from the joint fit. These results are shown in table 4, and are plotted against the joint fit $Y_{\rm sph}$ in figure 2. We found that the weighted mean of the ratio between the measurements is given by $Y_{\rm sph,SZ,B10}/Y_{sph} = 0.90 \pm 0.05$, where the uncertainty is the standard deviation of the weighted mean. A linear fit of the two measurements to a $y = x$ model results in $\chi^2_{\rm min} = 35.3$ for 25 degrees of freedom, and we measure a scatter of 16%.

4.3. Comparison between the Bulbul et al (2010) and Arnaud et al (2010) pressure profiles applied to the SZ data

The SZA data were also fit to the Arnaud *et al* (2010) model using the same value of r_{500} as above. The best-fit parameters are shown in table 5. We compared the results from the Bulbul

Table 4. Best-fit parameters for the fit of the SZA data to the Bulbul *et al* (2010) average pressure model and integrated Y parameter out to r_{500}.

Cluster	P_{eo} (10^{-11} ergs cm^{-3})	R_s (arcsec)	$Y_{\mathrm{sph,SZ,B10}}$ (10^{-11})	$Y_{\mathrm{sph,SZ,B10}}/Y_{\mathrm{sph}}$ ratio
MACSJ0159.8 − 0849	$27.50^{+15.59}_{-8.64}$	$40.99^{+11.10}_{-9.58}$	$9.07^{+1.01}_{-0.96}$	0.94±0.23
Abell 383	$69.55^{+20.41}_{-18.33}$	$22.13^{+3.71}_{-2.71}$	$4.14^{+0.59}_{-0.54}$	0.99±0.29
MACS0329.7 − 0212	$342.00^{+164.70}_{-189.90}$	$8.58^{+3.80}_{-1.42}$	$2.65^{+0.40}_{-0.37}$	1.02±0.32
Abell 478	$29.21^{+9.36}_{-2.84}$	$112.80^{+16.68}_{-30.96}$	$70.98^{+14.10}_{-22.91}$	1.17±0.39
MACSJ0429.6 − 0253	$76.52^{+105.50}_{-49.91}$	$158.00^{+11.74}_{-5.10}$	$2.86^{+0.53}_{-0.45}$	0.87±0.29
3C186	$44.60^{+6.61}_{-3.33}$	$13.28^{+1.55}_{-1.65}$	$0.82^{+0.18}_{-0.19}$	0.95±0.32
MACSJ0744.9 + 3927	$45.46^{+46.37}_{-17.59}$	$29.91^{+13.04}_{-10.73}$	$5.50^{+0.90}_{-0.84}$	1.45±0.43
MACSJ0947.2 + 7623	$31.44^{+23.66}_{-12.82}$	$34.31^{+13.30}_{-9.49}$	$6.03^{+0.90}_{-0.98}$	1.01±0.31
Zwicky 3146	$103.20^{+39.66}_{-25.83}$	$25.36^{+4.43}_{-4.13}$	$11.89^{+1.43}_{-1.34}$	1.13±0.27
MACSJ1115.8 + 0129	$168.10^{+80.39}_{-49.95}$	$16.69^{+3.27}_{-2.90}$	$7.99^{+0.62}_{-0.58}$	1.28±0.30
MS1137.5 + 6625	$24.56^{+23.35}_{-9.57}$	$21.20^{+6.99}_{-6.27}$	$0.99^{+0.14}_{-0.15}$	1.36±0.37
Abell 1413	$12.53^{+2.33}_{-1.45}$	$147.10^{+44.37}_{-38.53}$	$45.11^{+18.10}_{-13.95}$	1.95±0.81
CLJ1226.9 + 3332	$140.50^{+78.93}_{-67.19}$	$129.00^{+5.15}_{-2.61}$	$3.28^{+0.34}_{-0.31}$	1.07±0.29
MACSJ1311.0 − 0311	$7.56^{+7.93}_{-5.26}$	$54.26^{+90.72}_{-21.33}$	$2.64^{+0.94}_{-0.94}$	1.14±0.47
RXJ1347.5 − 1145	$296.71^{+98.58}_{-58.19}$	$16.14^{+1.96}_{-2.20}$	$13.70^{+0.78}_{-0.82}$	0.63±0.13
Abell 1835	$53.08^{+18.43}_{-15.05}$	$47.82^{+11.38}_{-8.06}$	$28.70^{+3.90}_{-3.16}$	0.97±0.22
MACSJ1423.8 + 2404	$36.51^{+67.61}_{-24.81}$	$24.80^{+36.43}_{-11.04}$	$4.44^{+3.12}_{-1.42}$	1.76±1.03
MACSJ1427.3 + 4408	$90.97^{+53.49}_{-54.50}$	$13.51^{+8.13}_{-3.06}$	$2.26^{+0.54}_{-0.44}$	0.48±0.14
RXJ1504.1 − 0248	$159.80^{+141.20}_{-67.18}$	$22.95^{+7.81}_{-6.35}$	$12.91^{+2.25}_{-1.82}$	0.72±0.18
MACSJ1532.9 + 302	$44.70^{+69.13}_{-27.53}$	$28.87^{+28.77}_{-12.09}$	$5.72^{+1.83}_{-1.10}$	1.24±0.42
MACSJ1621.6 + 3810	$14.56^{+13.40}_{-4.74}$	$41.13^{+14.72}_{-14.84}$	$3.25^{+0.55}_{-0.57}$	1.18±0.35
Abell 2204	$34.12^{+6.11}_{-5.84}$	$89.47^{+16.45}_{-11.79}$	$59.98^{+9.65}_{-7.56}$	1.37±0.33
MACSJ1720.3 + 3536	$78.69^{+50.98}_{-29.90}$	$18.54^{+5.49}_{-4.26}$	$3.85^{+0.42}_{-0.39}$	0.98±0.24
RXJ2129.6 + 0005	$21.23^{+14.94}_{-8.42}$	$56.85^{+28.27}_{-16.83}$	$12.67^{+3.37}_{-2.34}$	1.21±0.38
Abell 2537	$15.75^{+8.35}_{-5.48}$	$55.18^{+22.51}_{-14.36}$	$8.74^{+1.99}_{-1.43}$	1.19±0.35

et al (2010) average pressure model with the Arnaud *et al* (2010) model in figure 3, and found very good agreement: the weighted average of the ratio between the Bulbul *et al* (2010) and the Arnaud *et al* (2010) models is 1.05 ± 0.06. A fit of the two measurements to a $y = x$ model assuming the values are independent results in an $\chi^2_{\mathrm{min}} = 5.6$ for 25 degrees of freedom, consistent with the presence of negligible scatter between the two measurements. The low value of χ^2_{min} is likely due to correlated errors, since the two measurements make use of the same data. Figure 4 shows the average Arnaud *et al* (2010) and Bulbul *et al* (2010) pressure profiles for our sample. The two parameterizations result in fits that are consistent at all radii within r_{500}. The consistency between the pressure profiles and the integrated $Y(r_{500})$ values measured from the two models indicates that the choice of parameterization for the gas pressure does not introduce a significant bias in the calculation of the integrated pressure within r_{500}.

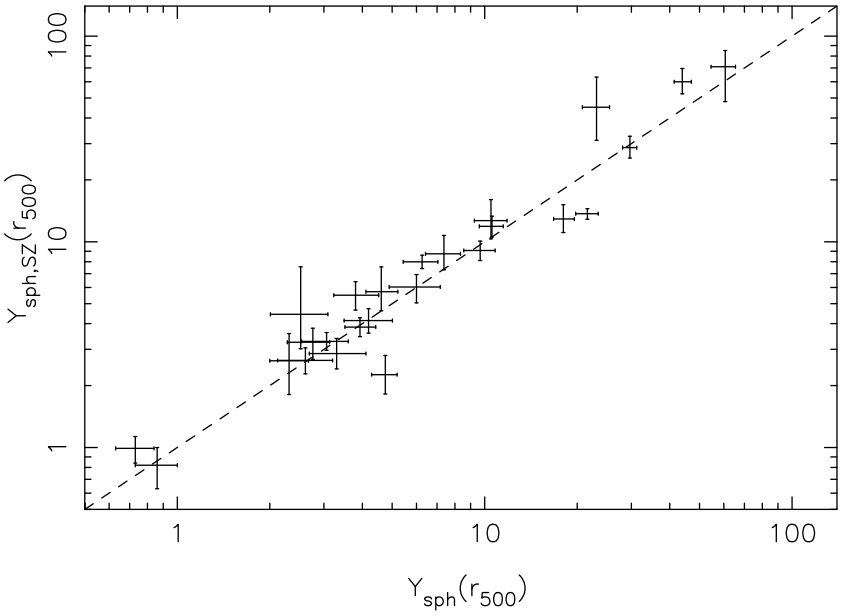

Figure 2. Integrated pressure ($Y_{\mathrm{sph,SZ,B10}}$) from SZ data plotted against integrated pressure (Y_{sph}) from the joint analysis, both measured out to the same value of r_{500}. The dashed line is the curve $y = x$.

5. Discussion

The agreement we found between SZ and x-ray measurements of the $Y_{\mathrm{sph}}(r_{500})$ parameter is consistent with a simple scenario in which the SZ decrement and the x-ray emission from massive relaxed clusters originate from the same highly ionized thermal plasma, with only small contributions from other possible sources of emission. This result is in agreement with earlier $\sim$30 GHz SZ studies using the Owens Valley Radio Observatory (OVRO) and the Berkeley Illinois Maryland Array (BIMA) millimeter arrays, in which the same value of the gas mass fraction was measured using SZ and x-ray data (LaRoque *et al* 2006). Our results also support the finding of Melin *et al* (2011) and Planck Collaboration *et al* (2011b) that there is overall agreement between the two measurements of the thermal pressure.

We found scatter between the SZA and *Chandra* Y_{sph} estimates at a level of 16%. A possible source of systematic error that could give rise to this scatter, and that is particularly relevant to our measurements out to r_{500}, is elongation of the cluster along the line of sight. We use spherically symmetric models in the analysis; an intrinsically prolate cluster (elongated along the line of sight), when fitted to a spherical model, will have its x-ray surface brightness—and therefore the corresponding Y_{sph} parameter—underestimated with respect to the corresponding SZ measurement (e.g. Cooray 2000, De Filippis *et al* 2005, Ameglio *et al* 2007). This is due to the quadratic dependence of the x-ray surface brightness profile on the density, as opposed to the linear dependence of the SZ effect. Our sample has just three clusters with a statistically significant deviation from the $Y_{\mathrm{sph}} = Y_{\mathrm{sph,SZ}}$ line, but in the direction of $Y_{\mathrm{sph}}/Y_{\mathrm{sph,SZ}} > 1$, and therefore consistent with oblateness (compression along the line of sight) rather than prolateness. The fact that the Allen *et al* (2008) sample of relaxed clusters is x-ray selected may lead to including preferentially oblate clusters as their surface brightness will be boosted. An

Table 5. Best-fit parameters for the fit of the SZA data to the Arnaud *et al* (2010) model and integrated Y parameter out to r_{500}.

Cluster	$p_{e,i}$ (10^{-11} ergs cm^{-3})	r_p ($''$)	$Y_{\mathrm{sph,SZ,A10}}$ (10^{-11})	$Y_{\mathrm{sph,SZ,B10}}/Y_{\mathrm{sph,SZ,A10}}$ ratio
MACSJ0159.8 − 0849	$6.38^{+2.71}_{-1.88}$	$221.0^{+56.9}_{-42.1}$	$9.16^{+1.21}_{-1.15}$	0.99±0.17
Abell 383	$48.1^{+101}_{-29.6}$	$74.0^{+37.7}_{-27.5}$	$2.93^{+0.71}_{-0.59}$	1.41 ± 0.37
MACS0329.7 − 0212	440^{+787}_{-328}	$25.0^{+17.7}_{-8.50}$	$2.01^{+0.46}_{-0.43}$	1.32±0.35
Abell 478	$7.50^{+1.43}_{-1.02}$	662.5^{+209}_{-153}	$93.9^{+48.3}_{-31.8}$	0.76 ± 0.42
MACSJ0429.6 − 0253	$3.50^{+5.01}_{-1.95}$	$206.7^{+161}_{-81.9}$	$3.61^{+0.96}_{-0.82}$	0.79±0.24
3C186	1570^{+609}_{-706}	$10.3^{+3.11}_{-1.26}$	$0.78^{+0.18}_{-0.14}$	1.05 ± 0.32
MACSJ0744.9 + 3927	$11.5^{+8.44}_{-4.34}$	$149.8^{+63.7}_{-44.2}$	$5.43^{+1.08}_{-0.93}$	1.01±0.25
MACSJ0947.2 + 7623	$6.68^{+5.66}_{-2.79}$	$195.0^{+81.4}_{-57.1}$	$6.10^{+1.23}_{-1.14}$	0.99±0.25
Zwicky 3146	$39.4^{+50.0}_{-21.0}$	$105.7^{+51.3}_{-33.9}$	$8.78^{+2.91}_{-2.02}$	1.35 ± 0.41
MACSJ1115.8 + 0129	$27.0^{+12.3}_{-7.88}$	$108.7^{+20.2}_{-17.8}$	$6.58^{+0.64}_{-0.60}$	1.21±0.15
MS1137.5 + 6625	$20.3^{+79.4}_{-14.5}$	$61.3^{+52.0}_{-30.2}$	$1.05^{+0.16}_{-0.18}$	0.94±0.21
Abell 1413	$4.11^{+0.77}_{-0.54}$	619.0^{+231}_{-167}	$42.8^{+21.8}_{-15.8}$	1.06±0.60
CLJ1226.9 + 3332	$35.9^{+43.5}_{-19.0}$	$67.6^{+30.2}_{-20.3}$	$3.07^{+0.43}_{-0.40}$	1.07±0.18
MACSJ1311.0 − 0311	709^{+2240}_{-641}	$16.2^{+24.7}_{-7.56}$	$0.99^{+0.58}_{-0.42}$	2.67±1.62
RXJ1347.5 − 1145	$50.7^{+9.85}_{-7.97}$	$102.7^{+9.48}_{-8.91}$	$13.0^{+0.82}_{-0.80}$	1.06±0.09
Abell 1835	$14.7^{+3.77}_{-3.11}$	$230.6^{+36.3}_{-29.8}$	$25.1^{+3.34}_{-2.94}$	1.14±0.20
MACSJ1423.8 + 2404	$7.82^{+24.9}_{-5.44}$	$137.8^{+239}_{-75.2}$	$4.20^{+4.57}_{-1.97}$	1.06±0.98
MACSJ1427.3 + 4408	$15.9^{+32.4}_{-10.1}$	$84.6^{+58.5}_{-34.3}$	$2.18^{+0.62}_{-0.51}$	1.04±0.35
RXJ1504.1 − 0248	$30.7^{+18.9}_{-11.0}$	$136.6^{+36.1}_{-28.9}$	$11.7^{+2.31}_{-1.85}$	1.10±0.29
MACSJ1532.9 + 302	$12.8^{+9.26}_{-4.87}$	$135.8^{+48.2}_{-36.3}$	$5.03^{+1.21}_{-0.99}$	1.14±0.38
MACSJ1621.6 + 3810	$4.78^{+2.74}_{-1.59}$	$171.9^{+61.1}_{-43.5}$	$3.00^{+0.57}_{-0.54}$	1.08±0.27
Abell 2204	$9.88^{+1.85}_{-1.51}$	$416.4^{+72.8}_{-59.0}$	$54.7^{+11.2}_{-8.98}$	1.10±0.26
MACSJ1720.3 + 3536	$13.1^{+5.22}_{-3.52}$	$119.5^{+22.2}_{-19.4}$	$3.89^{+0.41}_{-0.41}$	0.99±0.15
RXJ2129.6 + 0005	$4.50^{+2.45}_{-1.39}$	$328.6^{+128}_{-89.2}$	$13.3^{+3.80}_{-2.98}$	0.95±0.32
Abell 2537	$4.63^{+2.29}_{-1.37}$	$250.6^{+80.5}_{-59.4}$	$8.07^{+1.87}_{-1.54}$	1.08±0.31

alternative interpretation for the presence of scatter between the SZA and *Chandra* estimates of Y is that some of these clusters are disturbed and have undergone a recent merger, as is almost certainly the case for RXJ1347.5 − 1145 (Mason *et al* 2010, Johnson *et al* 2011). A merger would result in clumping of the gas and therefore an overstimate of the gas mass and Y from x-ray measurements, as suggested by Simionescu *et al* (2011) to explain the observations of the Perseus cluster. Clumping would not affect the SZ observations, because of the linear dependence of the signal on density.

The fit of the SZ data to the universal pressure profile of Arnaud *et al* (2010), and to the average pressure profile based on the Bulbul *et al* (2010) parameterization of the pressure, is statistically acceptable for all clusters, with a similar χ^2 for the two models. The agreement between Y_{sph} at r_{500} using the two models indicates that the integrated pressure is not highly sensitive to (reasonable) choices of parameterization.

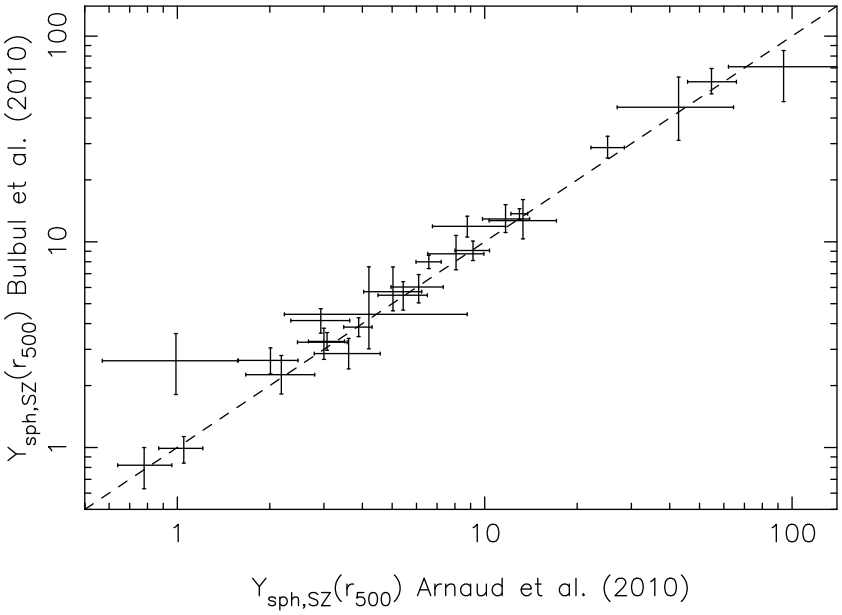

Figure 3. Integrated SZ pressure $Y_{\mathrm{sph,SZ}}$ calculated using the Bulbul *et al* (2010) model (y-axis) and the Arnaud *et al* (2010) model (x-axis), from a fit to the SZ data. The value of r_{500} was determined by the joint modeling of the SZ and x-ray observations, and it is the same for both measurements. The dashed line is the curve $y = x$.

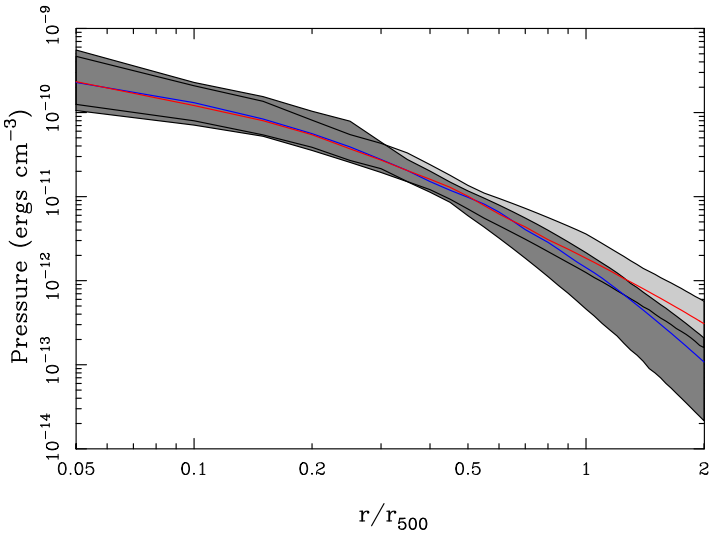

Figure 4. Average pressure profiles from SZ fits to Bulbul *et al* (2010) model (dark gray area, blue line) and to the Arnaud *et al* (2010) model (light gray area, red line). The lines are the median of the 25 best-fit distributions, and the error bands are the 68% confidence level.

We have adopted throughout our analysis the value of r_{500} determined from the joint SZ and x-ray observations. In the absence of x-ray information, one may instead adopt a fiducial value of the gas mass fraction f_{gas} to determine r_{500} (e.g. Joy *et al* 2001, Bonamente

et al 2008, Mroczkowski 2011) or other means based on SZ–mass scaling relations. The additional assumptions required for estimating r_{500} from SZ data will probably only contribute additional scatter to the $Y_{\rm sph} - Y_{\rm sph,SZ}$ relation when the r_{500} used to measure $Y_{\rm sph,SZ}$ is estimated directly from the SZ data.

6. Conclusions

We have presented a joint analysis of the SZA and *Chandra* observations of the Allen *et al* (2008) sample of massive and relaxed galaxy clusters. We have collected sensitive SZ data for all clusters at declination $\geqslant -15^{\circ}$ with no significant contamination from foreground or intrinsic radio sources, for a total of 25 clusters in the redshift range $0.09 \leqslant z \leqslant 1.06$. We also used the x-ray imaging and spectroscopic *Chandra* data that are available for all clusters, and made a cluster-by-cluster comparison of the integrated pressure. The $Y_{\rm sph}$ value estimated from the joint SZ and x-ray data, and from the SZ data alone, agree within a few per cent at r_{500}, indicating that the SZ and x-ray signal from massive relaxed clusters is consistent with a common thermal origin. We therefore confirm the findings of Melin *et al* (2011) and Planck Collaboration *et al* (2011b), and find no evidence for the presence of significant sources of systematic uncertainty in the measurements of the ICM pressure from the SZ and x-ray observations of massive relaxed clusters.

We also determined an average pressure profile based on the Bulbul *et al* (2010) model, with shape parameters ($n = 3.5$ and $\beta = 2.0$) determined by a joint fit to the *Chandra* x-ray data and our SZA observations of the Allen *et al* (2008) sample of massive relaxed clusters. We have shown that measurements of the radial profile of the pressure out to r_{500}, and of $Y_{\rm sph,SZ}$ at r_{500}, agree between the Arnaud *et al* (2010) and the Bulbul *et al* (2010) average pressure profiles out to r_{500}. Our conclusions indicate that both models are adequate for describing cluster radial pressure profiles and measuring the integrated thermal energy content in relaxed clusters.

Acknowledgments

The operation of the SZA is supported by the NSF through grants AST-0604982 and AST-0838187. Partial support was also provided by grant PHY-0114422 of the University of Chicago and by NSF grants AST-0507545 and AST-05-07161 to Columbia University. The CARMA operations are supported by the NSF under a cooperative agreement and by the CARMA partner universities. Support for TM was provided by the NASA through Einstein Postdoctoral Fellowship grant number PF0-110077 awarded by the Chandra X-ray Center, which is operated by the Smithsonian Astrophysical Observatory for NASA under contract NAS8-03060.

References

Allen S W, Rapetti D A, Schmidt R W, Ebeling H, Morris R G and Fabian A C 2008 *Mon. Not. R. Astron. Soc.* **383** 879

Ameglio S, Borgani S, Pierpaoli E and Dolag K 2007 *Mon. Not. R. Astron. Soc.* **382** 397

Arnaud M, Pratt G W, Piffaretti R, Böhringer H, Croston J H and Pointecouteau E 2010 *Astron. Astrophys.* **517** A92

Atrio-Barandela F, Kashlinsky A, Kocevski D and Ebeling H 2008 *Astrophys. J. Lett.* **675** L57

Bielby R M and Shanks T 2007 *Mon. Not. R. Astron. Soc.* **382** 1196

Birkinshaw M, Hughes J P and Arnaud K A 1991 *Astrophys. J.* **379** 466
Bonamente M, Joy M, LaRoque S J, Carlstrom J E, Nagai D and Marrone D P 2008 *Astrophys. J.* **675** 106
Bonamente M, Joy M K, Carlstrom J E, Reese E D and LaRoque S J 2004 *Astrophys. J.* **614** 194
Bonamente M, Joy M K, LaRoque S J, Carlstrom J E, Reese E D and Dawson K S 2006 *Astrophys. J.* **647** 25
Bulbul G E, Hasler N, Bonamente M and Joy M 2010 *Astrophys. J.* **720** 1038
Carlstrom J E, Holder G P and Reese E D 2002 *Annu. Rev. Astron. Astrophys.* **40** 643
Carlstrom J E, Joy M and Grego L 1996 *Astrophys. J. Lett.* **456** L75
Cooray A R 2000 *Mon. Not. R. Astron. Soc.* **313** 783
De Filippis E, Sereno M, Bautz M W and Longo G 2005 *Astrophys. J.* **625** 108
Diego J M and Partridge B 2010 *Mon. Not. R. Astron. Soc.* **402** 1179
Holzapfel W L, Arnaud M, Ade P A R, Church S E, Fischer M L, Mauskopf P D, Rephaeli Y, Wilbanks T M and Lange A E 1997 *Astrophys. J.* **480** 449
Johnson R E, ZuHone J A, Jones C, Forman W and Markevitch M 2011 arXiv:1106.3489J
Joy M, LaRoque S, Grego L, Carlstrom J E, Dawson K, Ebeling H, Holzapfel W L, Nagai D and Reese E 2001 *Astrophys. J.* **551** L1
Komatsu E *et al* 2011 *Astrophys. J. Suppl.* **192** 18
LaRoque S J, Bonamente M, Carlstrom J E, Joy M K, Nagai D, Reese E D and Dawson K S 2006 *Astrophys. J.* **652** 917
Lieu R, Mittaz J P D and Zhang S-N 2006 *Astrophys. J.* **648** 176
Marriage T A *et al* 2011 *Astrophys. J.* **737** 61
Mason B S *et al* 2010 *Astrophys. J.* **716** 739
Mazzotta P, Rasia E, Moscardini L and Tormen G 2004 *Mon. Not. R. Astron. Soc.* **354** 10
Melin J-B, Bartlett J G, Delabrouille J, Arnaud M, Piffaretti R and Pratt G W 2011 *Astron. Astrophys.* **525** A139+
Mroczkowski T 2011 *Astrophys. J. Lett.* **728** L35
Mroczkowski T *et al* 2009 *Astrophys. J.* **694** 1034
Muchovej S *et al* 2010 *Astrophys. J.* **716** 521
Nagai D, Vikhlinin A and Kravtsov A V 2007 *Astrophys. J.* **655** 98
Navarro J F, Frenk C S and White S D M 1997 *Astrophys. J.* **490** 493
Planck Collaboration (Ade P A *et al*) 2011a *Astron. Astrophys.* **536** A8
Planck Collaboration (Aghanim N *et al*) 2011b *Astron. Astrophys.* **536** A10
Reese E D, Carlstrom J E, Joy M, Mohr J J, Grego L and Holzapfel W L 2002 *Astrophys. J.* **581** 53
Simionescu A *et al* 2011 *Science* **331** 1576
Sunyaev R A and Zel'dovich Y B 1972 *Comments Astrophys. Space Phys.* **4** 173
Vanderlinde K *et al* 2010 *Astrophys. J.* **722** 1180
Vikhlinin A, Kravtsov A, Forman W, Jones C, Markevitch M, Murray S S and Van Speybroeck L 2006 *Astrophys. J.* **640** 691
Williamson R *et al* 2011 *Astrophys. J.* **738** 139